Since January 2020 Elsevier has created a COVID-19 resource centre with free information in English and Mandarin on the novel coronavirus COVID-19. The COVID-19 resource centre is hosted on Elsevier Connect, the company's public news and information website.

Virology 553 (2021) 35–45

Contents lists available at ScienceDirect

Virology

journal homepage: www.elsevier.com/locate/virology

Development and utilization of an infectious clone for porcine deltacoronavirus strain USA/IL/2014/026

Xufang Deng [a,*], Alexandra C. Buckley [b], Angela Pillatzki [c], Kelly M. Lager [b], Susan C. Baker [a], Kay S. Faaberg [b,**]

[a] Department of Microbiology and Immunology, Loyola University Chicago, Stritch School of Medicine, Maywood, IL, 60153, USA
[b] Virus and Prion Research Unit, USDA-ARS-National Animal Disease Center, Ames, IA, 50010, USA
[c] Animal Disease Research & Diagnostic Laboratory, South Dakota State University, Brookings, SD, 57007, USA

ARTICLE INFO

Keywords:
Porcine deltacoronavirus
Coronavirus infectious clone
Enteric coronavirus
Coronavirus pathogenesis
Endoribonuclease
NS6
Interferon antagonist
Infection of piglets

ABSTRACT

We report the generation of a full-length infectious cDNA clone for porcine deltacoronavirus strain USA/IL/2014/026. Similar to the parental strain, the infectious clone virus (icPDCoV) replicated efficiently in cell culture and caused mild clinical symptoms in piglets. To investigate putative viral interferon (IFN) antagonists, we generated two mutant viruses: a nonstructural protein 15 mutant virus that encodes a catalytically-inactive endoribonuclease (icEnUmut), and an accessory gene NS6-deletion virus in which the NS6 gene was replaced with the mNeonGreen sequence (icDelNS6/nG). By infecting PK1 cells with these recombinant PDCoVs, we found that icDelNS6/nG elicited similar levels of type I IFN responses as icPDCoV, however icEnUmut stimulated robust type I IFN responses, demonstrating that the deltacoronavirus endoribonuclease, but not NS6, functions as an IFN antagonist in PK1 cells. Collectively, the construction of a full-length infectious clone and the identification of an IFN-antagonistic endoribonuclease will aid in the development of live-attenuated deltacoronavirus vaccines.

1. Introduction

Coronaviruses (CoVs) are infamous for their ability to transmit across species from zoonotic reservoirs to humans and domestic animals, as exemplified by the human pathogens severe acute respiratory syndrome (SARS) CoV, Middle East respiratory syndrome (MERS) CoV and the ongoing COVID-19 pandemic caused by SARS-CoV-2 (de Wit et al., 2016; Perlman and Netland, 2009; Zhou et al., 2020). The family *Coronaviridae*, subfamily *Orthocoronavirinae*, of the order *Nidovirales* has been genetically divided into four genera: alpha, beta, gamma, and delta (https://ictv.global/taxonomy). Alpha (α) - and beta (β) - CoVs genetically derive from bat CoVs and mainly infect mammals. Gamma (γ) - and delta (δ) - CoVs are genetically related to bird CoVs. Unlike γ-CoVs primarily infecting birds, δ-CoVs have been found to infect both birds and mammals (Woo et al., 2012).

Six porcine CoVs have been identified to date: four α-CoVs [Transmissible gastroenteritis virus (TGEV), porcine respiratory coronavirus (PRCoV), porcine epidemic diarrhea virus (PEDV), and swine acute diarrhea syndrome coronavirus (SADS-CoV, also known as swine enteric alphacoronavirus)], one β-CoV [porcine haemagglutinating encephalomyelitis virus (PHEV)], and one δ-CoV [porcine deltacoronavirus (PDCoV)] (Wang et al., 2019). PDCoV was first reported in 2012 in China and placed in a new CoV genera, along with δ-CoVs of other mammals and birds (Woo et al., 2012). There is now evidence that the virus has been circulating in China since 2004, and it has been identified as an enteric pathogen of swine in several countries (Dong et al., 2015; Lee and Lee, 2014; Li et al., 2014; Wang et al., 2014). In the USA, PDCoV was first detected in 2014, and is now known to be present since the fall of 2013 (Sinha et al., 2015). PDCoV infection causes an age-dependent gastroenteritis with symptoms of acute diarrhea and dehydration seen in neonatal pigs (Jung et al., 2016; Zhang, 2016). It primarily spreads in the swine population but can also experimentally infect calves and chickens, possibly due to its broad receptor usage (Boley et al., 2020; Jung et al., 2017; Li et al., 2018). This highlights the potential for CoV diverse cross-species transmission.

The PDCoV genome is a single-stranded, positive-sense RNA of

* Corresponding author.
** Corresponding author.
E-mail addresses: xudeng@luc.edu (X. Deng), kay.faaberg@usda.gov (K.S. Faaberg).

https://doi.org/10.1016/j.virol.2020.11.002
Received 25 September 2020; Received in revised form 9 November 2020; Accepted 10 November 2020
Available online 13 November 2020

approximately 25 kb in length with the genome organization of δ-CoVs: 5′-UTR-ORF1a/1b-S-E-M-NS6-N-NS7-NS7a-3′UTR. The ORF1a/1b encodes two large replicase precursor polyproteins, pp1a and pp1ab, with the expression of the latter via a −1 ribosomal frameshift mechanism. Based on sequence comparison to other CoVs, the polyprotein pp1a and pp1ab of δ-CoV are autocatalytically processed to yield 15 nonstructural proteins (nsps) by two viral proteases that reside in pp1a. The N-terminus of δ-CoV pp1a/1 ab lacks sequence that is similar to the nsp1 regions of α- and β-CoVs (Narayanan et al., 2015). The nsps possess essential functions required for viral RNA synthesis and modulating host cellular responses. The nsp15 proteins of α- and β-CoVs retain an endoribonuclease (EndoU) activity and function as interferon (IFN) antagonists that mediate the evasion of host sensing by removing viral pattern recognition signatures from viral RNAs (Deng et al., 2017; Hackbart et al., 2020; Kindler et al., 2017). Whether the nsp15 of δ-CoV acts in a similar manner as its counterparts in other CoVs requires investigation. The last third of the genome codes for four structural proteins [spike (S), envelope (E), membrane (M), nucleocapsid (N)], and two nonstructural accessory proteins, NS6 and NS7. An additional accessory protein identical to the 3′ end of NS7 (100 aa), termed NS7a, was shown to be encoded by a separate subgenomic mRNA with a non-canonical transcription regulatory sequence (TRS) (Fang et al., 2017). The four structural proteins are required for the assembly of infectious viral particles. The functions of NS6, NS7, and NS7a remain unclear. One study reported that recombinant PDCoV with the ATG of NS7 removed had no diminishing effect on strain CHN-HG-2017 virulence and that NS6 could be replaced by a green fluorescent protein (GFP) with a reduction in clinical signs, yet no sequence verification after inoculation into swine was completed to fully understand the underlying genetic basis for the phenotype (Zhang et al., 2020). Another study reported that NS6 could antagonize IFN-β production when it was ectopically expressed (Fang et al., 2018). The proposed IFN antagonism of NS6 needs to be validated during PDCoV infection.

In this report, we describe the generation a reverse genetic tool for PDCoV strain USA/IL/2014/026 and the manipulation of icPDCoV to further understand the role of nsp15 and NS6 in δ-CoV replication.

2. Results

PDCoV infectious clone characteristics. An infectious cDNA clone of wild-type PDCoV was prepared and transcribed *in vitro* into genomic viral RNA as detailed in the Materials and Methods section and as shown in Fig. 1. Initially, obvious cytopathic effect (CPE) after electroporation of PK1 cells was not observed, nor was CPE detected in cells incubated with the supernatant from the electroporated cells. However, viral leader-containing subgenomic mRNA from the total RNA extracted from the electroporated cells was detected using RT-PCR (data not shown), indicating transcription of viral RNA was occurring. This lack of CPE for the PDCoV infectious clone may have been due to inadequate cell adaptation of a newly isolated PDCoV field strain, as a similar phenomenon was reported for porcine epidemic diarrhea virus (Deng et al., 2019; Hou et al., 2018). In order to obtain adaptive mutations that would allow for efficient recovery of PDCoV in cell culture, the PDCoV parental strain was passaged thirty times in PK1 cells. A growth curve analysis showed that the 30th passage (P30) virus propagated to a peak titer at an earlier time and at a higher titer than the first passage (P1) virus (Fig. 2A), suggesting that the virus was adapting to replicate in PK1 cells. The viral RNA (vRNA) was isolated from P1 and P30 viruses and the complete genomes of both vRNA populations were sequenced. A total of six single nucleotide substitutions that resulted in six amino acid mutations were detected in the genomic sequences of P30 as compared to P1 genome (Fig. 2B). Four of the six mutations were within the glycoprotein spike sequence, one was located in nonstructural protein 12 (nsp12), and one in the envelope gene (Fig. 2B and C). We reasoned that the spike mutations might facilitate PDCoV adaptation, as the spike protein is a major player in coronavirus entry and cell tropism. Therefore, the four spike mutations (H236Y, V441F, I550L, and L566Q) were engineered into the full-length cDNA clone, designated icP30, and tested for recovery of infectious virus that could induce CPE. As anticipated, CPE was detected 24 h post-electroporation (Fig. 2D). Next, in order to minimize the number of mutations in the spike region and to find out which mutation was sufficient for inducing CPE, we made a series of E subclones that contained either three spike mutations (H236Y, V441F, and I550L), or two (H236Y and V441F), or only one mutation (H236Y). The H236Y mutation alone, an externally facing residue on the globular head of the spike protein, was sufficient for recombinant PDCoV to cause CPE in PK1 cells (Fig. 2D). Hence, this recombinant PDCoV was designated icPDCoV.

Characterization of icPDCoV. To characterize the recombinant virus, a plaque assay determined that both the wild-type parental virus (Parental) and icPDCoV formed plaques with a similar size in PK1 cells (Fig. 3A). To verify the sequence of Parental and icPDCoV, the genomic regions harboring a Sap I restriction site (T_{20143}-to-A) in the parental strain and absent in icPDCoV were amplified and the RT-PCR fragments were subjected to Sap I digestion. As expected, the RT-PCR fragment amplified from the parental virus was digested by the Sap I enzyme,

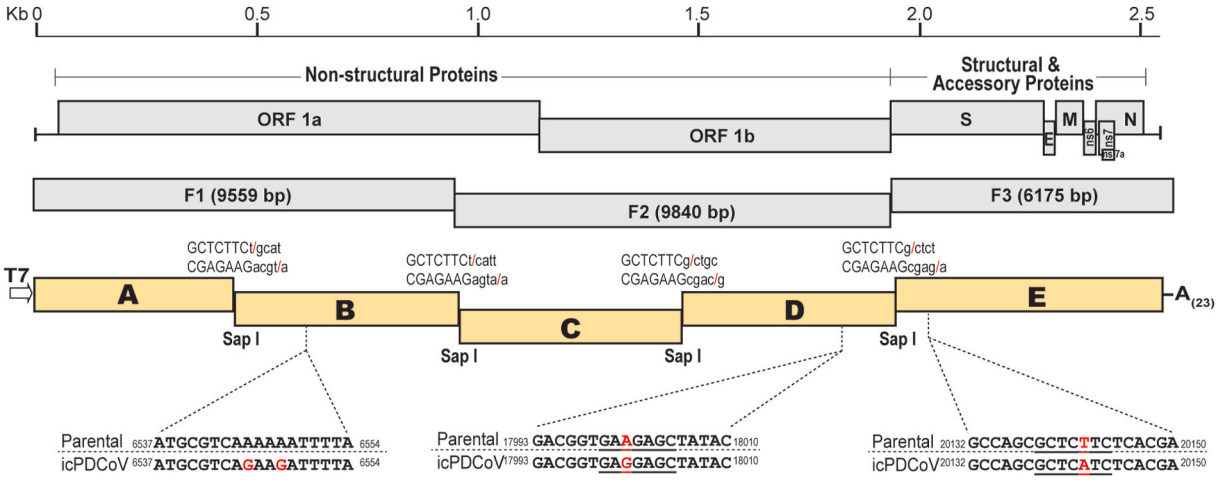

Fig. 1. Schematic diagram of the strategy used to generate an infectious clone of the USA/IL/2014 strain of PDCoV. The gene order of PDCoV is 5′-UTR-ORF1a/1b-S-E-M-NS6-N-NS7/7a-3′-UTR. Two third of the genome encodes a non-structural polyprotein while the rest of genome encodes structural and accessory proteins. Three DNA fragments (F1–F3) encompassing the entire genome were synthesized and used as template for the amplification of five DNA segments (A–E). Restriction enzyme sites used for directional ligation and the intentional nucleotide substitutions described in this study are depicted.

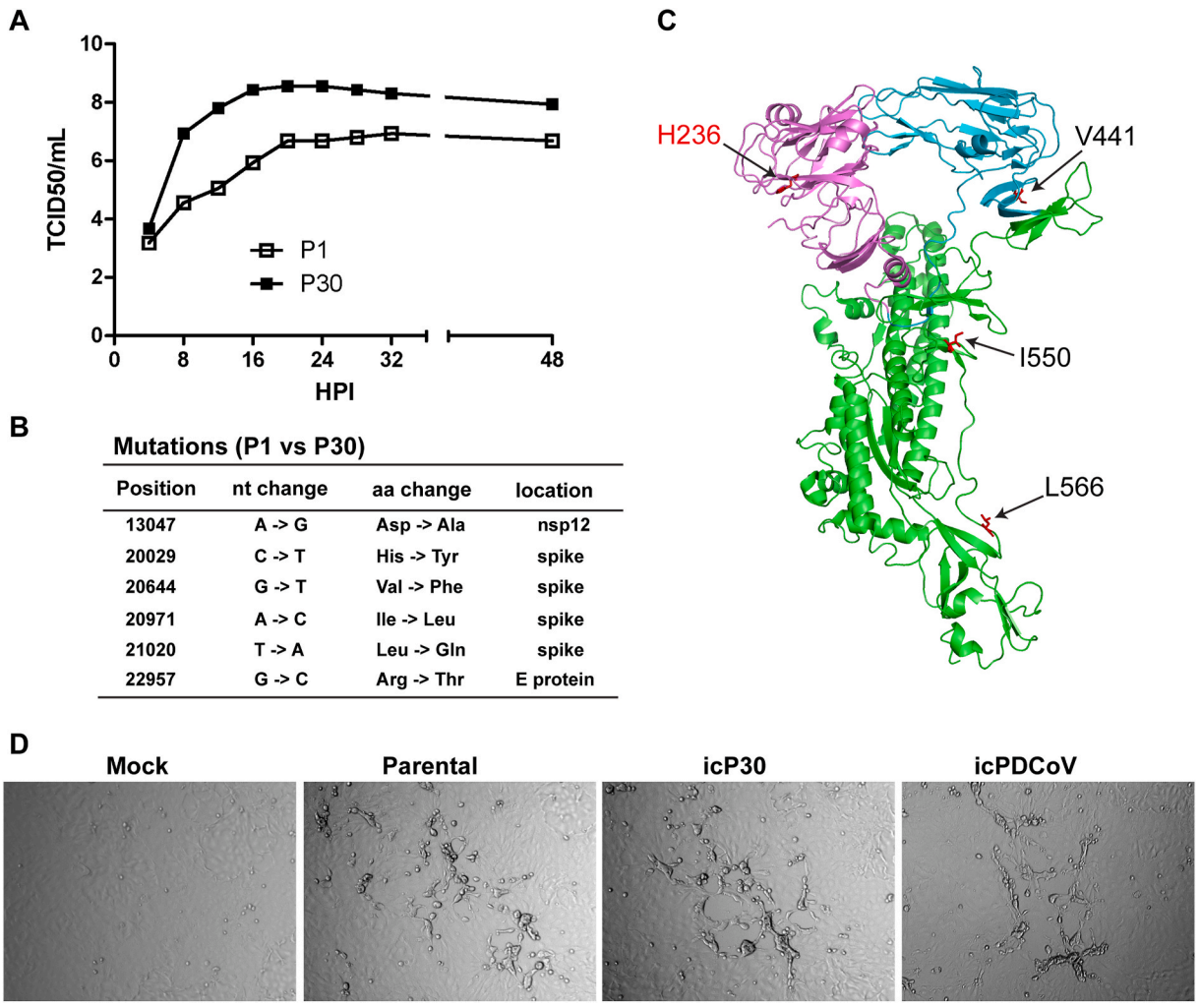

Mutations (P1 vs P30)

Position	nt change	aa change	location
13047	A -> G	Asp -> Ala	nsp12
20029	C -> T	His -> Tyr	spike
20644	G -> T	Val -> Phe	spike
20971	A -> C	Ile -> Leu	spike
21020	T -> A	Leu -> Gln	spike
22957	G -> C	Arg -> Thr	E protein

Fig. 2. Adaptive mutations allow rescue of infectious PDCoV that produces observable cytopathic effect in PK1 cells. In order to obtain cell culture adaptive mutation(s), the parental strain (P1) was passaged for 30 times (P30) in PK1 cells. (A) Growth kinetics analysis of P1 and P30 indicates P30 grew more rapidly and reached peak titer earlier than P1. (B) Full-genome sequencing revealed six nonsynonymous nucleotide substitutions in the genome of the P30 virus. (C) Four of the six substitutions reside in the spike sequence and are indicated in the protein structure of PDCoV spike (PDB#: 6b7n). (D) Incorporating all four (icP30) or one (H236Y) of the spike substitutions (icPDCoV) allows the recovered infectious clone virus to produce CPE in PK1 cells.

while the RT-PCR product derived from icPDCoV was resistant to Sap I-digestion (Fig. 3B). We further performed whole-genome sequencing on a plaque-purified icPDCoV clone and confirmed the fidelity of the genomic sequence (accession number: MW196362). To characterize their replication in cell culture, both the parental and icPDCoV were used to infect PK1 cells, and the extracellular titers in the cell culture supernatants were determined. As shown in Fig. 3C, the growth kinetics of icPDCoV is similar to that of the parental strain and both viruses replicate to peak titers at 48 h post-infection (hpi). In addition, the expression of the nucleocapsid (N) protein was detected in PK1 cells that were infected with either the parental or icPDCoV using an indirect immunofluorescence assay with a specific N protein monoclonal antibody (Fig. 3D).

Evaluating the replication and pathogenesis of the parental strain and recombinant PDCoV in conventional piglets. To investigate the replication and pathogenesis of icPDCoV in comparison with the parental strain, sixteen 5–7 day old piglets were orally inoculated with either the parental strain (n = 8) or icPDCoV (n = 8) at a dose of 10^5 TCID50 per animal. During the 21 days of infection, both groups of animals infected with either the parental strain or icPDCoV exhibited negligible or mild clinical symptoms. Only a few piglets of each group had loose stool or transient mild diarrhea at 2–4 day post-infection (dpi) (data not shown). Control animals were healthy and showed no sign of disease through the entire infection course. Although the virus-infected piglets exhibited mild clinical symptoms, we detected high and comparable levels of viral RNA in the rectal swabs (Fig. 4A). The peak viral RNA level (~10^8 copies/mL) was detected between 6 and 8 dpi. To assess the antibody response to infection, sera were collected at 21 dpi and subjected to a fluorescence-linked immunosorbent assay (FLISA) to detect virus-specific IgG titer. As shown in Fig. 4B, sera collected from both virus-infected challenge groups have high titers of virus-specific IgG with a similar mean of 400–500 fold dilution.

Histopathological examination and immunohistochemistry were performed on sections of small intestines from two pigs that were euthanized from each group at 4 and 7 dpi. At 4 dpi, all examined intestinal sections exhibited normal histology with no lesions identified. At 7 dpi, lesions consisted of villus atrophy and fusion, contraction of superficial villus lamina, and vacuolar degeneration, necrosis, and attenuation and sloughing of villus tip enterocytes observed in the sections of both infected groups, but not in the control animals. Lesions were present in both jejunum and ileum sections from all infected pigs. Lesion severity was not significantly different in infected pigs between the two virus-infected groups; however, individual variation was observed in both groups. Representative images of ileum sections from an age-matched, uninfected piglet and from one piglet per virus-infected group are shown in Fig. 5A. To determine if the sites of virus replication

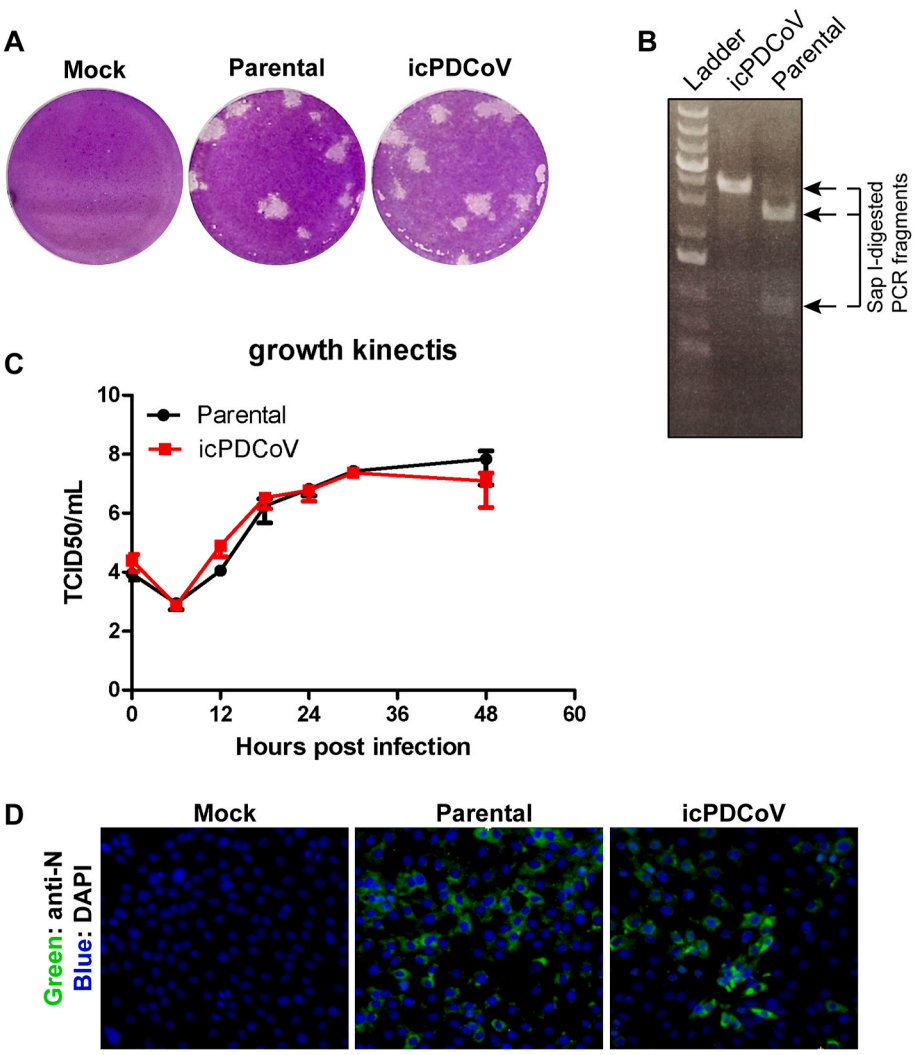

Fig. 3. Characterization of the rescued PDCoV from the infectious clone. (A) Representative plaques of mock-, the parental strain-, and icPDCoV-infected LLC-PK1 cells at 40 h post-infection. (B) PCR fragment amplified from the parental virus was digested by the Sap I enzyme, while the PCR product derived from icPDCoV was resistant to Sap I-digestion. (C) Growth kinetics of the parental strain (Parental) and infectious clone strain (icPDCoV) in PK1 cells. (D) Detection of N protein expression in parental- or icPDCoV-infected PK1 cells using an immunofluorescence assay with a mouse *anti*-N monoclonal antibody.

were similar in all infected animals, immunohistochemistry to detect PDCoV N protein was completed. Similar to previous studies (Chen et al., 2015; Jung et al., 2015), viral N protein was mainly detected in epithelial cells, and no apparent differences in the sites of replication of both viral strains were observed (Fig. 5B). These results collectively indicate that icPDCoV replicated as efficiently as the parental strain in piglets and caused mild disease.

Utilization of icPDCoV. A full-length infectious clone is a useful reverse genetic tool for studying the biology of a virus. In order to identify viral interferon antagonists of PDCoV, we targeted two viral proteins: endoribonuclease (EndoU) and accessory protein NS6. The endoribonucleases of α- and β-CoVs have been previously shown to be a potent IFN antagonist (Deng et al, 2017, 2019; Kindler et al., 2017). It is unknown if δ-CoV-encoded EndoU possesses a similar function. NS6 has been reported to suppress the type I IFN response when it was ectopically expressed in cell culture, but whether it acts as an IFN antagonist during virus infection remains unclear (Fang et al., 2018). To this end, we generated two mutant icPDCoVs (Fig. 6A): 1) icEnUmut, a mutant virus expressing an inactive EndoU in which a conserved catalytic histidine residue was mutated to an alanine (H219A); 2) icDelNS6/nG, a recombinant icPDCoV where the ns6 gene was replaced with the coding sequence of a mNeonGreen (nGreen) protein. Both mutant viruses were successfully rescued and the incorporated nucleotide sequence changes confirmed by Sanger sequencing. To characterize these mutant viruses, a plaque assay and a growth kinetics assay were performed. As shown in Fig. 6B, while icEnUmut formed slightly smaller size of plaques compared to icPDCoV, icDelNS6/nG produced relative uniform but markedly reduced size of plaques compared to the other two viruses, suggesting that the replacement of ns6 gene with a NeonGreen sequence greatly reduced viral replication. The growth kinetics analysis showed that icPDCoV replicated robustly and peaked at 24 hpi with a titer of near 10^8 $TCID_{50}$/mL. In contrast, both mutant viruses had lower titers than icPDCoV at all tested post-infection time points with a peak titer of below 10^6 $TCID_{50}$/mL (Fig. 6C). The expression of nGreen during infection was observed in icDelNS6/nG-infected PK1 cells under a fluorescence microscope (Fig. 6D). The N protein expression of icPDCoV and two mutant viruses was analyzed in a western blotting assay (Fig. 6E). Both mutant viruses had a lower expression of N protein compared to that of icPDCoV at 18 and 24 hpi, reflecting the result of the growth kinetic analysis.

To determine if PDCoV EndoU and NS6 function as IFN antagonists during infection, we evaluated the type I IFN responses by RT-qPCR in PK1 cells upon PDCoV infection. As shown in Fig. 7, icEnUmut-infected cells expressed higher mRNA levels of IFN-β (Fig. 7A) and IFN-stimulated genes (ISGs) (Fig. 7B) but a lower level of N gene in comparison with icPDCoV-infected cells. The relatively low expression of N mRNA in icEnUmut-infected cells may be due to the increased IFN-β and ISGs expression that suppressed ongoing viral replication. These results were consistent with the observations obtained from other EndoU mutant viruses (Deng et al, 2017, 2019; Kindler et al., 2017) and indicate that the EndoU of PDCoV is an IFN antagonist. Interestingly, unlike a PEDV EndoU mutant virus that elicited a higher level of TNF-α than its

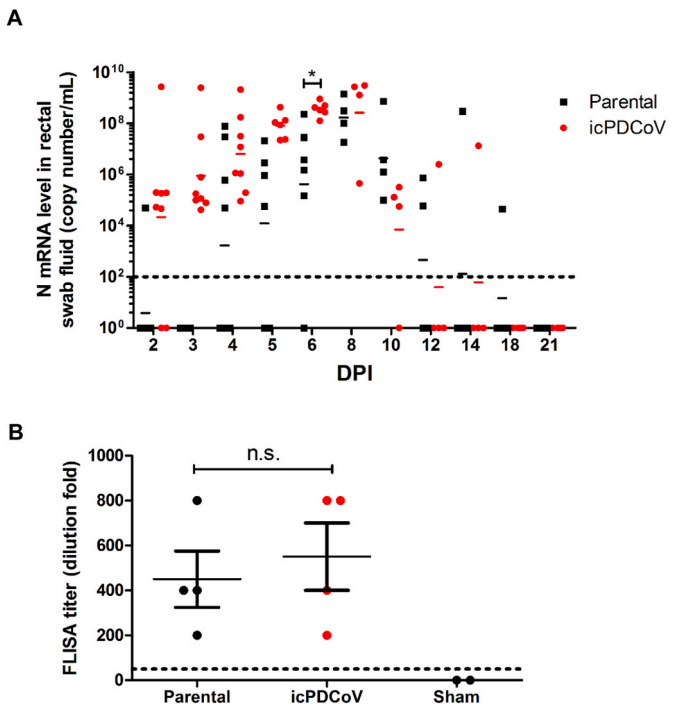

Fig. 4. Evaluating viral replication and the virus-specific IgG response to PDCoV infection. 5~7-day-old piglets were orally inoculated with either the parental strain or infectious clone PDCoV at a dose of 10^5 $TCID_{50}$ per pig. (A) RT-qPCR was performed on fecal swab samples that were taken at the indicated time points in a 21-day infection course. The bars represent the geometric means of N gene copy numbers of the animal group on a specific day. (B) The titer of PDCoV-specific IgG in serum samples was measured using FLISA (see details in Materials and Methods). Unpaired t tests were used in (A) and (B). Error bars represent mean ± SEM. *, $p < 0.05$; n.s., not significant.

isogenic wild-type virus (Deng et al., 2019), icEnUmut stimulated a similar level of TNF-α as icPDCoV (Fig. 7B), suggesting a uniqueness of PDCoV EndoU. In contrast to icEnUmut, icDelNS6/nG-infected cells had lower levels of IFN-β and ISGs and N gene expression (Fig. 7A and B). The low N gene level of icDelNS6/nG reflects the growth kinetics and western blotting results (Fig. 6C and E) and is likely due to impaired viral replication caused by the insertion of a foreign gene (Zhang et al., 2020). Even though the impaired viral replication may delay the induction of IFN-β and ISGs, similar IFN-β mRNA levels were observed (16 hpi of icPDCoV vs 24 hpi of icDelNS6/nG) when both viruses had comparable levels of N gene at these time points (Fig. 6). These results together suggested that the removal of the ns6 gene does not affect the ability of the virus to inhibit the type I IFN responses, and replacing ns6 with a mNeonGreen sequence likely resulted in a replication defect.

3. Discussion

We constructed a full-length infectious cDNA clone for PDCoV strain USA/IL/2014/026 and demonstrated its usefulness to mine the genome for potential virulence factors. Recently, Zhang et al. reported a reverse genetic system for a PDCoV Chinese strain CHN-HG-2017 using a similar strategy (Zhang et al., 2020). While the PDCoV USA strain in the present study caused a mild disease in piglets, the Chinese strain and the recombinant PDCoV were pathogenic in 5-day-old piglets and caused various degrees of clinical symptoms (Zhang et al., 2020). The differences in pathogenicity of both the Chinese strain and the USA strain might be due to the experimental settings such as different infection doses (10^7 $TCID_{50}$ versus 10^5 $TCID_{50}$ per pig in our study) and the age of animals. Besides, genomic sequence analysis reveals that the Chinese strain and the USA strain share 98.8% nucleotide identity, with 311 nucleotide differences evenly scattered throughout the genome. When accessing the spike glycoprotein region only, the two PDCoV strains share 97.1% amino acid identity, with most differences noted within the S1 domain. In addition, the S1 protein of strain USA/IL/2014/026 harbors two less putative N-glycan sequons and contains an extra asparagine residue when compared to Chinese strain CHN-HG-2017. Lastly, when completing phylogeny analysis on complete genome sequences of PDCoV, CHN-HG-2017 was found to group within a different lineage than USA/IL/2014/026 (data not shown). The differences noted may have an effect on strain virulence and can now be investigated using our reverse genetic system for PDCoV.

PDCoV causes age-dependent diarrhea in piglets. Eleven to 14 day-old gnotobiotic pigs were susceptible to high dose oral infection of the OH-FD22 strain [8.8 log_{10} genomic equivalents (GEs) or 10.8 log_{10} GEs] or OH-FD100 (11.0 log_{10} GEs), resulting in acute, severe, watery diarrhea and/or vomiting at 21–24 h post-inoculation (Hu et al., 2016; Jung et al., 2015). Chen et al. reported that orally inoculating 5-day-old conventional piglets (3×10^4 $TCID_{50}$ per pig) with the USA/IL/2014 strain resulted in diarrheal disease at day 5 post-infection with macro- and microscopic lesions, but no other clinical symptoms (Chen et al., 2015). In our study, USA/IL/2014 orally infected 5–7 day old piglets again exhibited very mild symptoms, confirming the presence of both PDCoV and icPDCoV disease, and the same clinical outcome that was observed previously using USA/IL/2014 (Chen et al., 2015). A FLISA was also established, showing equivalent amounts of serum IgG was elicited by icPDCoV and the parental strain infection.

The function of the coronaviral endoribonuclease has been shown to be important for evading multiple host dsRNA sensors, including melanoma differentiation-associated protein 5 (MDA5), protein kinase R (PKR) and 2′-5′-oligoadenylate synthetase (OAS) [reviewed in (Deng and Baker, 2018)]. Sequence alignment from all four CoV genera and structural analysis showed that δ-CoV EnU contains the key residues that are required for endoribonuclease activity (Deng and Baker, 2018; Zheng et al., 2018). As shown for EndoUs of mouse hepatitis virus, human coronavirus 229E, SARS-CoV-2, and PEDV, PDCoV EndoU may also interfere with host innate immunity (Deng et al, 2017, 2019; Kindler et al., 2017; Yuen et al., 2020). We provide *in vitro* evidence that PDCoV EndoU/nsp15 acts as an IFN antagonist. At 24 hpi, icPDCoV replicated 100-fold higher than icEnUmut in the interferon-responsive PK1 cell line (Fig. 6C), and the comparative levels of intracellular IFN-β, ISGs, and PDCoV N gene RNA were consistent with EndoU/nsp15 preventing the activation of host innate immune responses (Fig. 7).

δ-CoV NS6 is an accessory protein that is encoded by ORF6. Previous studies have shown that PDCoV NS6 primarily localizes in the cytoplasm of infected PK1 cells and, when overexpressed, inhibits the expression of IFN-β in Sendai virus infected HEK-293T cells by curbing the interaction between RIG-I/MDA5 and double-stranded RNA (Fang et al, 2016, 2018). Whether NS6 functions as an IFN antagonist when in the context of PDCoV infection was not clear. Recently, PDCoV NS6 was exchanged for GFP (ΔNS6-GFP) in a reverse genetics system for strain CHN-HG-2017 (Zhang et al., 2020). After infection of 5-day old piglets with the wild-type recombinant PDCoV (rPDCoV-wt) or ΔNS6-GFP, fecal shedding was assessed as well as viral RNA load and comparative IL-1β, TNF-α and IL-6 transcripts in the duodenum, jejunum and ileum at 4 dpi. All results pointed to decreased fecal shedding, decreased expression of cytokines and virus by ΔNS6-GFP virus when compared to rPDCoV-wt. The authors determined that the disruption of NS6 impaired viral replication and the virus was attenuated in piglets. However, whether NS6 directly impaired the type I IFN response was not addressed. In order to provide additional clarity to the question of the role of NS6 in PDCoV, we replaced NS6 by mNeonGreen to produce icDelNS6/nG. Upon infection of PK1 cells, icDelNS6/nG replicated 100-fold less than icPDCoV but did not elicit robust levels of IFN-β nor ISGs (Fig. 7). These results suggest that NS6 does not act as an IFN antagonist during PDCoV infection.

To conclude, a reverse genetics system was devised and developed

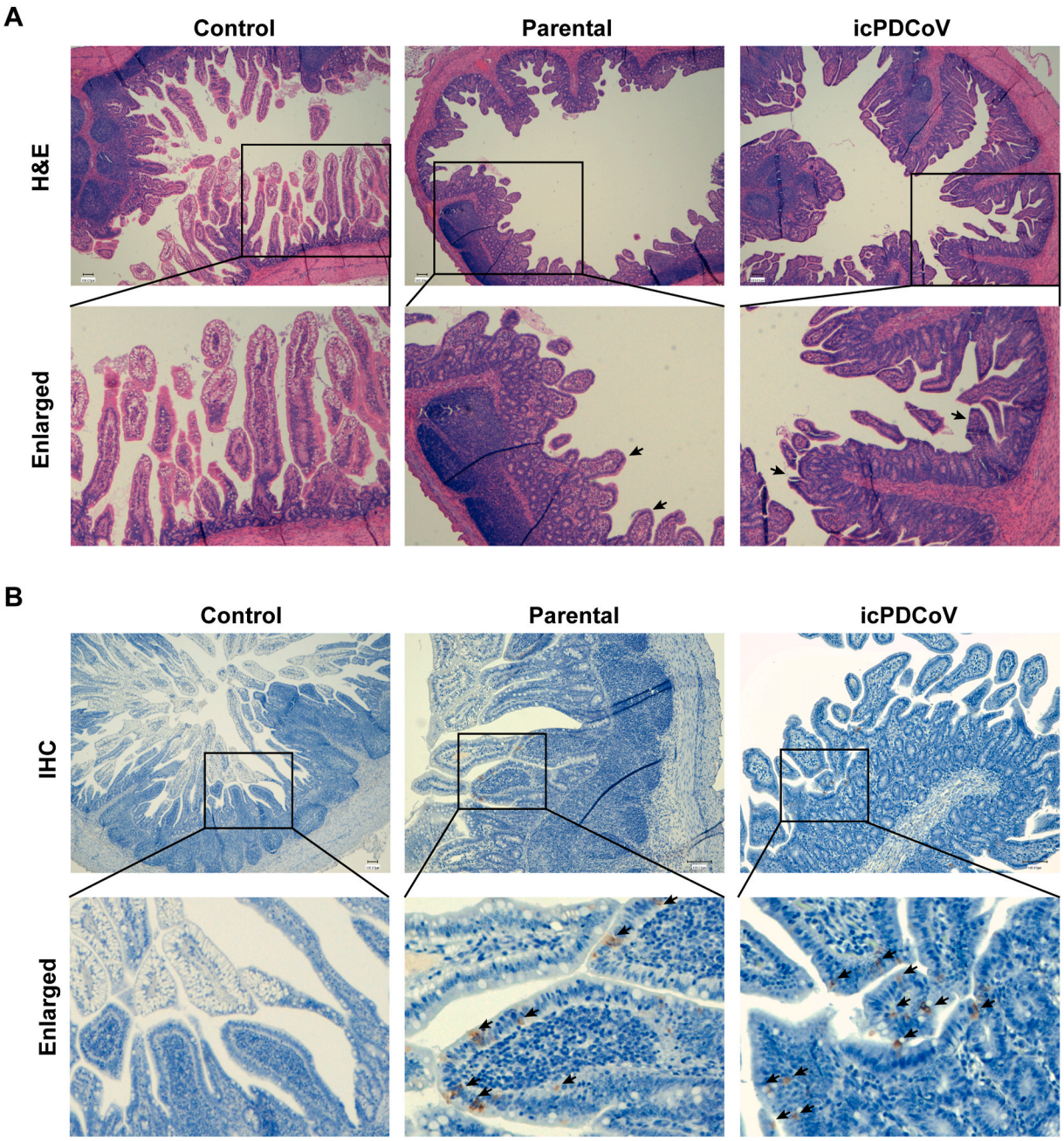

Fig. 5. Histology and immunohistochemistry staining of uninfected control, parental PDCoV-, and icPDCoV-infected piglet ileum. (A) Representative images of H&E stained histological sections of ileum specimens collected at day 7 post-infection (upper panel, 4 × ; lower panel, enlarged). Representative lesions (shortened villi and damaged mucosal epithelial cells, etc) are indicated by arrows. (B) Immunohistochemistry (IHC) staining of ileum specimens collected at day 4 post-infection (upper panel, 4 × ; lower panel, enlarged) using a mouse *anti*-PDCoV-N antibody. The brown-coloration indicates PDCoV-positive epithelial cells, which are identified by arrows. (For interpretation of the references to color in this figure legend, the reader is referred to the Web version of this article.)

for USA strain IL/2014/026 (icPDCoV). Two mutants were also produced, one where the active site residue for EndoU in nsp15 was substituted for alanine (icEnUmut) and one in which the NS6 protein was replaced by mNeonGreen (icDelNS6/nG). After infection of PK1 cells, we confirmed the IFN-β inhibition by parental PDCoV nsp15, but found that the replacement of NS6 by mNeonGreen had no effect on the low IFN-β levels seen with icPDCoV. icPDCoV and the mutants provide a necessary tool for future investigation of δ-CoV pathogenesis.

4. Methods and materials

Virus and cells. Porcine kidney epithelial cells, LLC-PK1 (ATCC, CL-101), termed PK1 cells, were purchased from ATCC and grown in growth medium containing modified Eagle medium (MEM) (Corning, 10010-CV) supplemented with heat-inactivated 5% fetal calf serum (FCS) (Atlanta Biological) and 1% penicillin/streptomycin (pen/strep; HyClone). The PDCoV USA/IL/2014/026 strain (Lot # 026PDV1402) was obtained from the USDA National Veterinary Services Laboratories (NVSL) and was propagated once in PK1 cells to make a large stock. This viral stock was defined as the parental PDCoV strain and used through the study. Maintenance medium contains MEM supplemented with 0.3% tryptose phosphate broth and 0.05% yeast extract.

Assembly of a full-length infectious clone. We used a published strategy to construct an infectious clone for PDCoV (Deng et al., 2019;

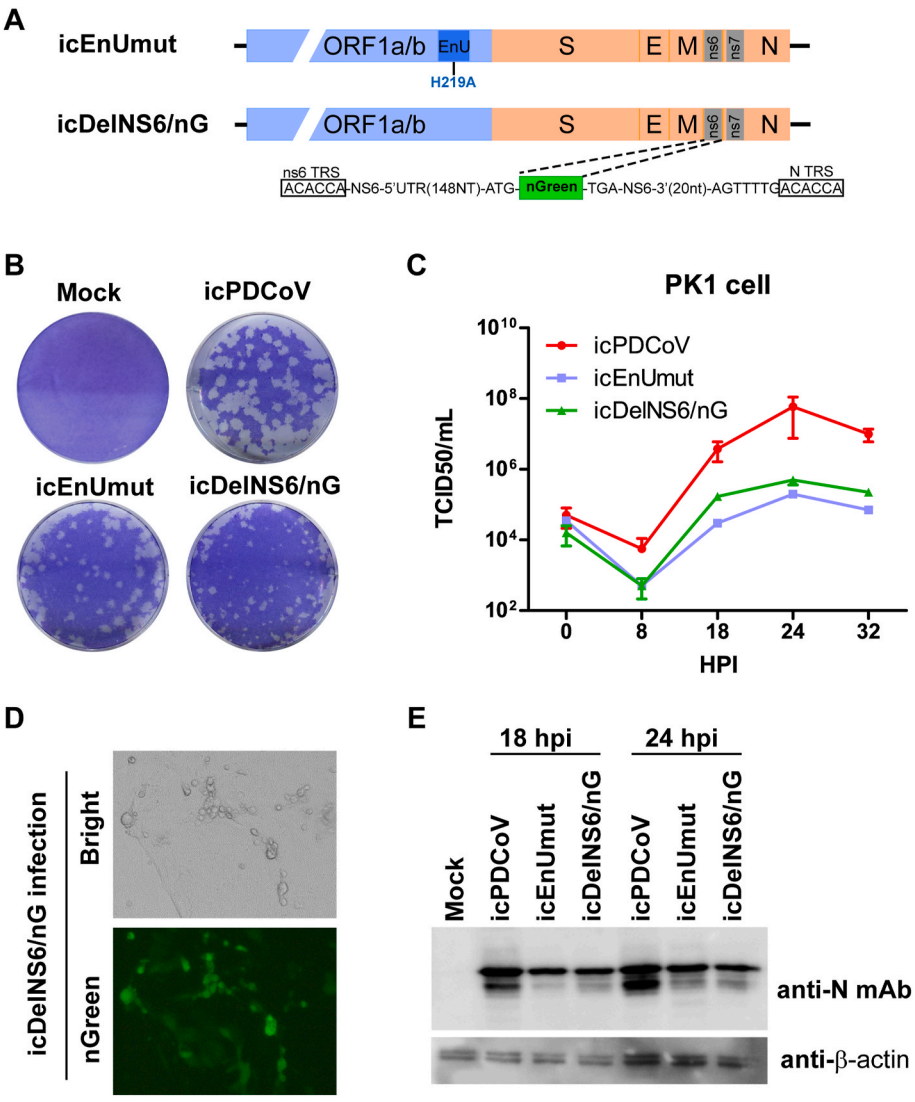

Fig. 6. Generation and characterization of PDCoV mutant viruses. (A) Two mutant PDCoVs were generated in this study. icEnUmut: Histidine-219 of the endoribonuclease (EndoU) of PDCoV was mutated to Alanine (H219A). icDelNS6/nG: the coding sequence of ns6 was replaced with neonGreen (nGreen) sequence. The TRS of ns6 and N gene are shown and boxed. A 20 nt coding sequence of ns6 at the 3′ end was retained to maintain the potential secondary structure of the TRS of N gene. (B) Representative plaques of the parental strain-, icPDCoV-, icEnUmut-, and icDelNS6/nG-infected PK1 cells at 32 h post-infection. (C) Growth kinetics of icPDCoV and mutant viruses. PK1 cells were infected at a dose of 0.1 $TCID_{50}$ per cell. Cell culture supernatant was collected at the indicated time points and subject to a $TCID_{50}$ assay in PK1 cells. Error bars represent mean ± standard deviation. (D) icDelNS6/nG infection in PK1 cells caused CPE (Bright) and yielded green signal (nGreen) under a fluorescence microscope. (E) Western blotting detection of the expression of N protein using mouse *anti*-N monoclonal antibody (mAb). β-actin served as a loading control. (For interpretation of the references to color in this figure legend, the reader is referred to the Web version of this article.)

Yount et al., 2002). Briefly, three DNA fragments (F1 to F3) encompassing of the complete genomic sequence of a porcine deltacoronavirus USA/IL/2014/026 strain (GenBank accession number KP981395) were commercially synthesized (Genscript, NJ). These synthetic DNAs were used as the template for PCR amplification of five segments that were then cloned into plasmid vector backbones, designated PDCoV subclones A to E (Fig. 1). All subclones were joined by unique Sap I restriction endonuclease cleavage sites (at PDCoV nucleotide positions 4500, 9551, 14,575, and 19,396, respectively) that allowed for directional assembly into a full-length cDNA without alteration of the viral amino acid sequence (Fig. 1). The promoter sequence of T7 RNA polymerase and a poly(A) tail (23 As) were added to the 5′ and 3’ ends of subclones A and E, respectively, allowing for generating capped and polyadenylated full-length transcripts using an *in vitro* RNA transcription reaction. In subclones D and E, two naturally occurring Sap I sites were removed by introducing silent mutations at positions 18,001 and 20,143, respectively. In subclone B, two silent mutations (A6545G and A6548G) were introduced to disrupt a stretch of six adenosine nucleotides that might interfere with *in vitro* RNA transcription. In addition, the coding sequence of the N gene was cloned into a pcDNA3.1 vector that carries a T7 promoter sequence. This recombinant N plasmid was used as a template for N gene RNA transcription.

To generate a PDCoV mutant virus expressing a catalytically inactive form of endoribonuclease, the histidine-219 of nsp15 was mutated to alanine (H219A) using site-directed mutagenesis on subclone D. To generate icDelNS6/nG, the coding sequence of mNeonGreen was synthesized (Genscript, NJ) and inserted into the subclone E to replace ns6 gene. Since the stop codon of ns6 gene is only 7 nucleotides upstream of the TRS of N gene, a 20 nt coding sequence at the 3’ end of ns6 was retained to minimize any potential adverse effects on the transcription of the N gene.

Recovery of recombinant virus. To recover infectious virus, the five PDCoV cDNA subclones were initially digested with Sap I and ligated *in vitro* using T4 DNA ligase. The ligated cDNA and a linearized N gene plasmid were purified and used as templates for *in vitro* T7 RNA transcription reactions to yield full-length genomic and N gene transcripts, respectively. These RNA transcripts were pooled together and electroporated into PK1 cells. To aid the recovery, the culture medium of the electroporated cells was replaced at 18 h post-electroporation with maintenance medium supplemented with 5 mg/L trypsin (Sigma, 59427C).

In order to obtain adaptive mutations, the parental PDCoV (P1) was serially passaged for thirty times in LLC-PK1 cells. Briefly, 5 μL of prior passaged viral stock was used to infect cells in a 60-mm dish. Cell culture supernatant containing cell-free viral particles was harvested as a new passage and used to infect fresh cells. After thirty passages, the passaged virus (P30) and P1 stock were subjected to a growth kinetic analysis and whole-genome sequencing (Kansas State Veterinary Diagnostic

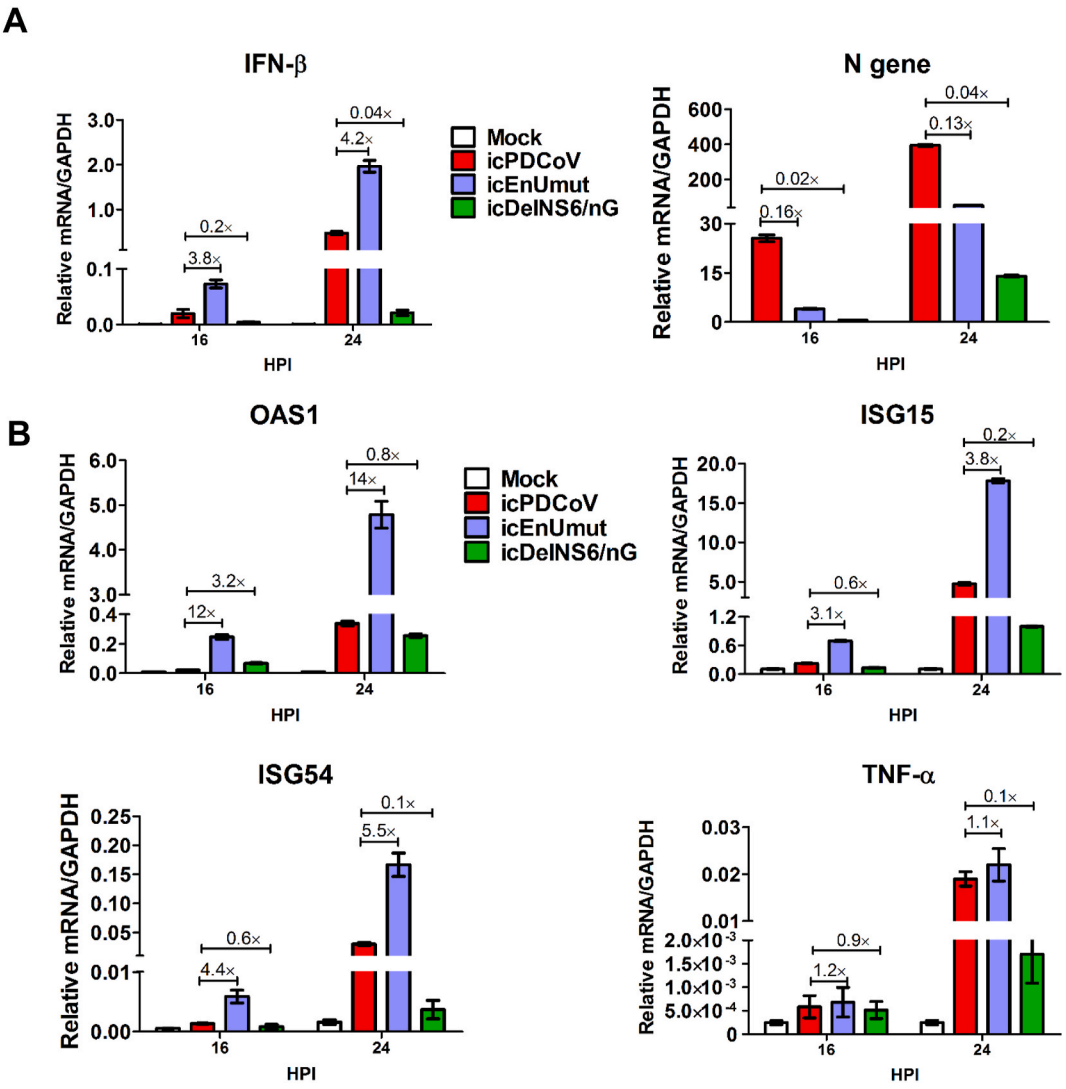

Fig. 7. Characterization of host immune responses in icPDCoV- and mutant viruses-infected PK1 cells. Cells were infected at a dose of 0.1 $TCID_{50}$ per cell and were harvested for total RNA extraction at indicated time points. The relative mRNA level of (A) IFN-β, N gene, (B) ISGs (OAS1, ISG15, ISG54), and TNF-α were measured using RT-qPCR. The experiment was performed three times, and the representative data are shown. Error bars represent mean ± SD and the relative fold-changes were shown above the error bars.

Laboratory, KS, USA). Nucleotide variations between P1 and P30 were identified via sequence alignment of both viruses' genomes. Subsequently, the non-synonymous variations within the spike gene were introduced into the infectious clone by site-direct mutagenesis and determined what variation(s) is sufficient for recombinant PDCoV to cause CPE.

Plaque assay. PK1 cells (3.0×10^5 cell per well) were plated in a 12-well or 6-well plate 24 h prior infection. Cells were washed twice with PBS and then infected with 10-fold serially diluted viral inoculum. After 1 h incubation, the inoculum was discarded and replaced with medium-agar (Oxoid, OXLP0028B) mixture (1:1 ratio) containing 5 μg/mL trypsin. After incubation for 32 or 40 h, the cells were fixed with 4% formaldehyde and stained with 0.5% crystal violet.

Growth kinetics and titration. In a 24-well (1.5×10^5 cells/well) plate, PK1 cells were infected with PDCoV at a dose of 0.1 $TCID_{50}$ per cell. After 1 h incubation, the inoculum was removed and replaced with the maintenance medium. Cell culture supernatant was collected at the indicated time points and subjected to titration using a $TCID_{50}$ assay. Briefly, PK1 cells seeded in a 96-well plate (4×10^4 cells/well) were washed twice with phosphate-buffered saline (PBS) and then incubated with serially 10-fold diluted supernatant collected from infected cells. The number of wells with visible CPE were counted 2 days post-infection. The $TCID_{50}$ value was calculated using the Reed-Muench method (Reed and Muench, 1938).

Fluorescence-linked immunosorbent assay (FLISA) and immunofluorescence assay (IFA). In a 96-well plate (for FLISA) or a 24-well plate (for IFA), PK1 cells were infected with icPDCoV or parental strain at a dose of 0.1 $TCID_{50}$ per cell. At 16 h post-infection, cells were washed once with PBS and fixed with cold methanol/acetone (50%/50%, vol/vol) for 15 min at −20 °C. Fixed cells were then blocked with PBS containing 5% FCS for 30 min at 37 °C and stained with mouse *anti*-N protein monoclonal antibody [mAb SD110-122 (Okda et al., 2016); courtesy of Eric A. Nelson, South Dakota State University] and goat anti-mouse IgG Alexa Fluor 488 (ThermoFisher, A-11001). Nuclei were visualized with Hoescht 33,342 (Life Technologies, H1339). Subsequently, cells were washed three times with PBS before examination using a fluorescence microscope. In order to determine the titer of virus-specific IgG with a FLISA, fixed cells were incubated with serially diluted pig serum for 1 h at 37 °C. Cells were washed three times with PBS and incubated with FITC-conjugated goat anti-swine IgG (H+L) secondary antibody (Southern Biotech, 6050-02). Subsequently, cells were washed three times with PBS before examination using a

fluorescence microscope.

Analysis of gene expression using RT-qPCR. To measure mRNA levels in cells, 3×10^5 PK1 cells per well were plated in a 12-well plate, 16 h prior to infection. Cells were washed twice with PBS and infected with the indicated virus at a dose of 0.1 $TCID_{50}$ per cell in the presence of 5 μg/mL trypsin. Cells were harvested at different time points using RLT buffer provided by the RNeasy mini kit (QIAGEN, 74,104) and total RNA was extracted as instructed by the manufacturer's protocol. 500 ng RNA was used for cDNA synthesis using the RT2 HT First Strand Kit (QIAGEN, 330,411). Quantitative PCR (qPCR) was performed using RT2 SYBR Green qPCR mix (QIAGEN, 330,502) in the Bio-Rad CFX96 system. The thermocycler was set as follows: one step at 95 °C (10 min), 40 cycles of 95 °C (15 s), 55 °C (1 min) and plate read, one step at 95 °C (10 s), and a melt curve from 65 °C to 95 °C at increments of 0.5 °C/0.05 s. Samples were assayed in triplicate and data are representative of three independent experiments. The levels of mRNA were relative to β-actin mRNA and expressed as $2^{-\Delta CT}$ [$\Delta CT = C_{T(gene\ of\ interest)} - C_{T(GAPDH)}$]. PCR primers used in this study are listed in Table 1.

Western blotting. PK1 cells (3.0×10^5 cell per well) in a 12-well plate were infected with indicated viral strains at a dose of 0.1 $TCID_{50}$ per cell and harvested with lysis buffer (20 mM Tris [pH 7.5], 150 mM NaCl, 1 mM EGTA, 1 mM EDTA, 1% Triton X-100, 2.5 mM sodium pyrophosphate, 1 mM β-glycerophosphate, 1 mM sodium orthovanadate, 1μg/ml leupeptin, 1 mM phenylmethylsulfonyl fluorid). Cell lysate was clarified by high-speed centrifugation and mixed with 5 × sample buffer (0.25 M Tris-HCl [pH 6.8], 0.5 M DTT, 10% SDS, 50% Glycerol, 0.5% bromphenol blue). 20 μL of lysate was separated by electrophoresis through a polyacrylamide gel and transferred onto a PVDF membrane. Mouse monoclonal antibodies against PDCoV N protein (mAb SD110-122) and β-actin (GenScript, A00702) were used to blot these proteins.

Animal experiment. Animal work was performed in accordance with the National Animal Disease Center (NADC) Animal Care and Use Protocol ARS-2017-603. Pregnant sows free of clinical disease and negative for PEDV and PDCoV antibodies via IFA were purchased from a commercial farm and transported to NADC prior to farrowing. Piglets were weaned from sows between 3 and 6 days of age. Piglets were blocked by litter and assigned to 3 treatment groups: icPDCoV (n = 8), PDCoV parental (n = 8), and controls (n = 8). Each group was housed in a separate biosafety level-2 animal room. Twenty-four hours after weaning, piglets were orally inoculated with 2 mL of virus solution at a titer of 10^5 $TCID_{50}$/pig. Control pigs received 2 mL of media inoculum orally. Piglets were rectal swabbed and the clinical diarrhea scores were recorded daily for 18 days. Clinical diarrhea scores were assigned with the following criteria: 0 = normal feces, 1 = soft stool, 2 = semi-liquid stool, 3 = liquid feces, 4 = voluminous watery diarrhea. Rectal swabs were collected with a sterile polyester-tipped applicator (Puritan Medical Products, Guilford, ME) immersed in 3 mL of serum-free MEM. Blood was collected in a serum separation tube (BD Vacutainer®, Franklin Lakes, NJ) and centrifuged to harvest serum on 0 and 21 dpi. Samples were stored at −80 °C until time of testing. Two piglets from each group were euthanized on 4 and 7 dpi for collection of jejunum and ileum tissue samples. Intestinal sections were fixed in 10% neutral buffered formalin and routinely processed. All remaining animals were euthanized on 21 dpi. Euthanasia was performed with an intravenous administration of barbiturate (Fatal Plus, Vortech Pharmaceuticals, Dearborn, MI) following the manufacturer labeled dose.

PDCoV RNA Quantification using Taqman Real Time PCR. Viral RNA was quantified from rectal swabs as previously described (Miller et al., 2016). Briefly, RNA extraction was performed using the MagMAX™ Pathogen RNA/DNA kit (catalog no. 4462359; Applied Biosystems) following manufacturer's recommendations for fecal samples. Viral RNA was eluted into 90 μL of elution buffer. Following extraction, 5 μL of the nucleic acid templates were added to 20 μL of the Path-ID™ Multiplex One-Step RT-PCR reaction master mix (catalog no. 4442137, Applied Biosystems). Real-time RT-PCR (RT-qPCR) was performed on an ABI 7500 Fast instrument run in standard mode with the following conditions: reverse transcription at 45 °C for 10 min and denaturation at 95 °C for 10 min, followed by 40 cycles of 95 °C for 15 s and 60 °C for 45 s. The primer and the probe were synthesized (Integrated DNA Technologies, Coralville, IA) and targeted a conserved region (nucleotides 372–441) of the PDCoV M gene with modifications specific to the PDCoV strain USA/IL/2014/026 (Table 1). PDCoV genome copies were calculated based on a standard RNA transcript overlapping the target region.

H&E staining and immunohistochemistry. The detail of this method was described previously (Deng et al., 2019). Briefly, tissues were fixed in neutral buffered formalin, processed, and embedded in paraffin. Five-micron-thick sections were cut and stained with hematoxylin and eosin (H&E) stain utilizing a Tissue-Tek automated slide stainer (Sakura Finetek USA, Torrence, CA). A veterinary pathologist who was blind to the treatment groups evaluated sections of small intestine by light microscopy to identify location and subjectively assess villus atrophy and crypt hyperplasia. For immunohistochemistry, the tissue sections were mounted on positively charged glass slides and oven dried for 60 min at 60 °C. Slides were deparaffinized and then rinsed three times in deionized water, followed by soaking in Tris buffer saline with Tween 20 for 5 min. Slides were placed in a Dako autostainer (Agilent, Santa Clara, CA) and run through a preprogrammed immunohistochemistry (IHC) protocol. The IHC protocol utilizes Protease XIV (Millipore Sigma, St. Louis, MO) for antigen retrieval, mouse monoclonal antibody SD110-122 specific for the nucleocapsid of PDCoV at 1:1000 dilution, Dako Envision+HRP (Agilent, Santa Clara, CA), and DAB substrate chromogen (Agilent, Santa Clara, CA). The slides were then counterstained in hematoxylin and cover slipped.

Data analysis and visualization. Experiments in the study were performed at least twice independently or with multiple biological replicates and representative results were presented. Numeric data were analyzed using appropriate statistical analyses described in corresponding figure legends and plotted using Graphpad Prism 7 (Graphpad, CA). Nucleotide and protein sequences were analyzed using Clone Manager Professional 9 (Sci Ed Software, CO).

Table 1
qPCR primers and probe sequences used in this study.

Method	Target	Forward (5'->3')	Reverse (5'->3')	Target Region (nucleotides)
SYBR Green	Porcine GAPDH	ACCTCCACTACATGGTCTACA	ATGACAAGCTTCCCGTTCTC	110-220
	Porcine IFN-β	AGCAGATCTTCGGCATTCTC	GTCATCCATCTGCCCATCAA	254-354
	Porcine ISG54	CTGGCAAAGAGCCCTAAGGA	CTCAGAGGGTCAATGGAATTCC	769-872
	Porcine ISG15	CCTGTTGATGGTGCAAAGCT	TGCACATAGGCTTGAGGTCA	210-436
	Porcine OAS1	AAGCATCAGAAGCTTTGCATCTT	CAGGCCTGGGTTTCTTGAGTT	790-889
	Porcine TNF-a	CCTACTGCACTTCGAGGTTATC	ACGGGCTTATCTGAGGTTTG	157-273
	PDCoV N gene	GTTACACCAGACAAAAGCCAG	ACCCTTAACCCAAGTAACACG	152-300
Taqman	PDCoV M gene	CGACCACATGGCTCCAATTC	CAGCTCTTGCCCATGTAGCTT	372-441
	M gene probe	FAM-CACACCAGTCG-ZEN-TTAAGCATGGCAAGC-Iowa Black[a]		

[a] FAM, 6-carboxyfluorescein.

Disclaimer

Mention of trade names or commercial products in this article is solely for the purpose of providing specific information and does not imply recommendation or endorsement by the U.S. Department of Agriculture. USDA is an equal opportunity provider and employer.

Declaration of competing interest

The authors have no competing interests to declare.

CRediT authorship contribution statement

Xufang Deng: Conceptualization, Data curation, Formal analysis, Investigation, Visualization, Methodology, Writing - original draft, Writing - review & editing. **Alexandra C. Buckley:** Conceptualization, Data curation, Formal analysis, Investigation, Methodology, Resources, Writing - review & editing. **Angela Pillatzki:** Investigation, Formal analysis, Methodology, Writing - review & editing. **Kelly M. Lager:** Project administration, Resources, Supervision, Funding acquisition, Writing - review & editing. **Susan C. Baker:** Funding acquisition, Project administration, Resources, Writing - review & editing. **Kay S. Faaberg:** Conceptualization, Funding acquisition, Project administration, Resources, Writing - original draft, Writing - review & editing.

Acknowledgements

We thank Jason Huegel, Justin Miller, Alyssa Dannen, Randy Leon, and Nate Horman, for providing animal care, as well as Deb Adolphson, Sarah Anderson and Miranda Dietz for technical assistance (animal handling, RT-qPCR). This work was funded by the USDA-Loyola University Chicago cooperative agreement #59-5030-8-003B, NIH AI085089 (to SCB), and USDA ARS CRIS Project 5030-32000-118-00D.

References

Boley, P.A., Alhamo, M.A., Lossie, G., Yadav, K.K., Vasquez-Lee, M., Saif, L.J., Kenney, S. P., 2020. Porcine deltacoronavirus infection and transmission in poultry, United States. Emerg. Infect. Dis. 26, 255–264. https://doi.org/10.3201/eid2602.190346.

Chen, Q., Gauger, P., Stafne, M., Thomas, J., Arruda, P., Burrough, E., Madson, D., Brodie, J., Magstadt, D., Derscheid, R., Welch, M., Zhang, J., 2015. Pathogenicity and pathogenesis of a United States porcine deltacoronavirus cell culture isolate in 5-day-old neonatal piglets. Virology 482, 51–59. https://doi.org/10.1016/J.VIROL.2015.03.024.

de Wit, E., van Doremalen, N., Falzarano, D., Munster, V.J., 2016. SARS and MERS: recent insights into emerging coronaviruses. Nat. Rev. Microbiol. 14, 523–534. https://doi.org/10.1038/nrmicro.2016.81.

Deng, X., Baker, S.C., 2018. An "Old" protein with a new story: coronavirus endoribonuclease is important for evading host antiviral defenses. Virology 517, 157–163. https://doi.org/10.1016/J.VIROL.2017.12.024.

Deng, X., Hackbart, M., Mettelman, R.C., O'Brien, A., Mielech, A.M., Yi, G., Kao, C.C., Baker, S.C., 2017. Coronavirus nonstructural protein 15 mediates evasion of dsRNA sensors and limits apoptosis in macrophages. Proc. Natl. Acad. Sci. U.S.A. 114, E4251–E4260. https://doi.org/10.1073/pnas.1618310114.

Deng, X., van Geelen, A., Buckley, A.C., O'Brien, A., Pillatzki, A., Lager, K.M., Faaberg, K. S., Baker, S.C., 2019. Coronavirus endoribonuclease activity in porcine epidemic diarrhea virus suppresses type I and type III interferon responses. J. Virol. 93, e02000–e02018. https://doi.org/10.1128/JVI.02000-18.

Dong, N., Fang, L., Zeng, S., Sun, Q., Chen, H., Xiao, S., 2015. Porcine deltacoronavirus in mainland China. Emerg. Infect. Dis. 21, 2254–2255. https://doi.org/10.3201/eid2112.150283.

Fang, P., Fang, L., Hong, Y., Liu, X., Dong, N., Ma, P., Bi, J., Wang, D., Xiao, S., 2017. Discovery of a novel accessory protein NS7a encoded by porcine deltacoronavirus. J. Gen. Virol. 98, 173–178. https://doi.org/10.1099/jgv.0.000690.

Fang, P., Fang, L., Liu, X., Hong, Y., Wang, Y., Dong, N., Ma, P., Bi, J., Wang, D., Xiao, S., 2016. Identification and subcellular localization of porcine deltacoronavirus accessory protein NS6. Virology 499, 170–177. https://doi.org/10.1016/j.virol.2016.09.015.

Fang, P., Fang, L., Ren, J., Hong, Y., Liu, X., Zhao, Y., Wang, D., Peng, G., Xiao, S., 2018. Porcine deltacoronavirus accessory protein NS6 antagonizes interferon beta production by interfering with the binding of RIG-I/MDA5 to double-stranded RNA. J. Virol. 92, e00712–e00718. https://doi.org/10.1128/JVI.00712-18.

Hackbart, M., Deng, X., Baker, S.C., 2020. Coronavirus endoribonuclease targets viral polyuridine sequences to evade activating host sensors. Proc. Natl. Acad. Sci. Unit. States Am. 117, 8094–8103. https://doi.org/10.1073/PNAS.1921485117.

Hou, Y., Meulia, T., Gao, X., Saif, L.J., Wang, Q., 2018. The deletion of both tyrosine-based endocytosis signal and endoplasmic reticulum-retrieval signal in the cytoplasmic tail of spike protein attenuates PEDV in pigs. J. Virol. https://doi.org/10.1128/JVI.01758-18. JVI.01758-18.

Hu, H., Jung, K., Vlasova, A.N., Saif, L.J., 2016. Experimental infection of gnotobiotic pigs with the cell-culture-adapted porcine deltacoronavirus strain OH-FD22. Arch. Virol. 161, 3421–3434. https://doi.org/10.1007/s00705-016-3056-8.

Jung, K., Hu, H., Eyerly, B., Lu, Z., Chepngeno, J., Saif, L.J., 2015. Pathogenicity of 2 porcine deltacoronavirus strains in gnotobiotic pigs. Emerg. Infect. Dis. 21, 650–654. https://doi.org/10.3201/eid2104.141859.

Jung, K., Hu, H., Saif, L.J., 2017. Calves are susceptible to infection with the newly emerged porcine deltacoronavirus, but not with the swine enteric alphacoronavirus, porcine epidemic diarrhea virus. Arch. Virol. 162, 2357–2362. https://doi.org/10.1007/s00705-017-3351-z.

Jung, K., Hu, H., Saif, L.J., 2016. Porcine deltacoronavirus infection: etiology, cell culture for virus isolation and propagation, molecular epidemiology and pathogenesis. Virus Res. 226, 50–59. https://doi.org/10.1016/j.virusres.2016.04.009.

Kindler, E., Gil-Cruz, C., Spanier, J., Li, Y., Wilhelm, J., Rabouw, H.H., Züst, R., Hwang, M., V'kovski, P., Stalder, H., Marti, S., Habjan, M., Cervantes-Barragan, L., Elliot, R., Karl, N., Gaughan, C., van Kuppeveld, F.J.M., Silverman, R.H., Keller, M., Ludewig, B., Bergmann, C.C., Ziebuhr, J., Weiss, S.R., Kalinke, U., Thiel, V., 2017. Early endonuclease-mediated evasion of RNA sensing ensures efficient coronavirus replication. PLoS Pathog. 13, e1006195 https://doi.org/10.1371/journal.ppat.1006195.

Lee, S., Lee, C., 2014. Complete Genome Characterization of Korean Porcine Deltacoronavirus Strain KOR/KNU14-04/2014. Genome Announc. vol. 2 https://doi.org/10.1128/genomeA.01191-14.

Li, G., Chen, Q., Harmon, K.M., Yoon, K.J., Schwartz, K.J., Hoogland, M.J., Gauger, P.C., Main, R.G., Zhang, J., 2014. Full-length genome sequence of porcine deltacoronavirus strain USA/IA/2014/8734. Genome Announc. 2, 278–292. https://doi.org/10.1128/genomeA.00278-14.

Li, W., Hulswit, R.J.G., Kenney, S.P., Widjaja, I., Jung, K., Alhamo, M.A., van Dieren, B., van Kuppeveld, F.J.M., Saif, L.J., Bosch, B.-J., 2018. Broad receptor engagement of an emerging global coronavirus may potentiate its diverse cross-species transmissibility. Proc. Natl. Acad. Sci. U.S.A. 115, E5135–E5143. https://doi.org/10.1073/pnas.1802879115.

Miller, L.C., Crawford, K.K., Lager, K.M., Kellner, S.G., Brockmeier, S.L., 2016. Evaluation of two real-time polymerase chain reaction assays for *Porcine epidemic diarrhea virus* (PEDV) to assess PEDV transmission in growing pigs. J. Vet. Diagn. Invest. 28, 20–29. https://doi.org/10.1177/1040638715621949.

Narayanan, K., Ramirez, S.I., Lokugamage, K.G., Makino, S., 2015. Coronavirus nonstructural protein 1: common and distinct functions in the regulation of host and viral gene expression. Virus Res. 202, 89–100. https://doi.org/10.1016/j.virusres.2014.11.019.

Okda, F., Lawson, S., Liu, X., Singrey, A., Clement, T., Hain, K., Nelson, J., Christopher-Hennings, J., Nelson, E.A., 2016. Development of monoclonal antibodies and serological assays including indirect ELISA and fluorescent microsphere immunoassays for diagnosis of porcine deltacoronavirus. BMC Vet. Res. 12, 95. https://doi.org/10.1186/s12917-016-0716-6.

Perlman, S., Netland, J., 2009. Coronaviruses post-SARS: update on replication and pathogenesis. Nat. Rev. Microbiol. 7 (6), 439–450. https://doi.org/10.1038/nrmicro2147.

Reed, L.J., Muench, H., 1938. A simple method of estimating fifty per cent endpoints. Am. J. Epidemiol. 27, 493–497. https://doi.org/10.1093/oxfordjournals.aje.a118408.

Sinha, A., Gauger, P., Zhang, J., Yoon, K.J., Harmon, K., 2015. PCR-based retrospective evaluation of diagnostic samples for emergence of porcine deltacoronavirus in US swine. Vet. Microbiol. 179, 296–298. https://doi.org/10.1016/j.vetmic.2015.06.005.

Wang, L., Byrum, B., Zhang, Y., 2014. Detection and genetic characterization of deltacoronavirus in pigs, Ohio, USA, 2014. Emerg. Infect. Dis. 20, 1227–1230. https://doi.org/10.3201/eid2007.140296.

Wang, Q., Vlasova, A.N., Kenney, S.P., Saif, L.J., 2019. Emerging and re-emerging coronaviruses in pigs. Curr. Opin. Virol. 34, 39–49. https://doi.org/10.1016/J.COVIRO.2018.12.001.

Woo, P.C.Y., Lau, S.K.P., Lam, C.S.F., Lau, C.C.Y., Tsang, A.K.L., Lau, J.H.N., Bai, R., Teng, J.L.L., Tsang, C.C.C., Wang, M., Zheng, B.-J., Chan, K.-H., Yuen, K.-Y., 2012. Discovery of seven novel mammalian and avian coronaviruses in the genus deltacoronavirus supports bat coronaviruses as the gene source of alphacoronavirus and betacoronavirus and avian coronaviruses as the gene source of gammacoronavirus and deltacoronavirus. J. Virol. 86, 3995–4008. https://doi.org/10.1128/JVI.06540-11.

Yount, B., Denison, M.R., Weiss, S.R., Ralph, S., Baric, R.S., 2002. Systematic assembly of a full-length infectious cDNA of mouse hepatitis virus strain A59. J. Virol. 76, 11065–11078. https://doi.org/10.1128/JVI.76.21.11065.

Yuen, C.K., Lam, J.Y., Wong, W.M., Mak, L.F., Wang, X., Chu, H., Cai, J.P., Jin, D.Y., To, K.K.W., Chan, J.F.W., Yuen, K.Y., Kok, K.H., 2020. SARS-CoV-2 nsp13, nsp14, nsp15 and orf6 function as potent interferon antagonists. Emerg. Microb. Infect. 9, 1418–1428. https://doi.org/10.1080/22221751.2020.1780953.

Zhang, J., 2016. Porcine deltacoronavirus: overview of infection dynamics, diagnostic methods, prevalence and genetic evolution. Virus Res. 226, 71–84. https://doi.org/10.1016/J.VIRUSRES.2016.05.028.

Zhang, M., Li, W., Zhou, P., Liu, D., Luo, R., Jongkaewwattana, A., He, Q., 2020. Genetic manipulation of porcine deltacoronavirus reveals insights into NS6 and NS7

functions: a novel strategy for vaccine design. Emerg. Microb. Infect. 9, 20–31. https://doi.org/10.1080/22221751.2019.1701391.

Zheng, A., Shi, Y., Shen, Z., Wang, G., Shi, J., Xiong, Q., Fang, L., Xiao, S., Fu, Z.F., Peng, G., 2018. Insight into the evolution of nidovirus endoribonuclease based on the finding that nsp15 from porcine Deltacoronavirus functions as a dimer. J. Biol. Chem. 293, 12054–12067. https://doi.org/10.1074/jbc.RA118.003756.

Zhou, P., Yang, X.-L., Wang, X.-G., Hu, B., Zhang, L., Zhang, W., Si, H.-R., Zhu, Y., Li, B., Huang, C.-L., Chen, H.-D., Chen, J., Luo, Y., Guo, H., Jiang, R.-D., Liu, M.-Q., Chen, Y., Shen, X.-R., Wang, X., Zheng, X.-S., Zhao, K., Chen, Q.-J., Deng, F., Liu, L.-L., Yan, B., Zhan, F.-X., Wang, Y.-Y., Xiao, G.-F., Shi, Z.-L., 2020. A pneumonia outbreak associated with a new coronavirus of probable bat origin. Nature 1–4. https://doi.org/10.1038/s41586-020-2012-7.